Electronic Supplementary Material (ESI) for ChemComm.
This journal is © The Royal Society of Chemistry 2020

Supporting Information:

Intrinsically low thermal conductivity in p-type semiconductor $SrOCuBiSe_2$ with a [SrO]-intercalated $CuBiSe_2$ structure

Mengjia Luo,[ab∇] Kejun Bu,[ab∇] Xian Zhang,*[c] Jian Huang,[a] Ruiqi Wang,[d] Fuqiang Huang*[ad]

[a.] *State Key Laboratory of High Performance Ceramics and Superfine Microstructure, Shanghai Institute of Ceramics, Chinese Academy of Sciences, Shanghai 200050, P.R. China;*

[b.] *University of Chinese Academy of Sciences, Beijing 100049, China;*

[c.] *Qian Xuesen Laboratory of Space Technology, China Academy of Space Technology, Beijing 100094, P. R. China. E-mail: zhangxian@qxslab.cn*

[d.] *State Key Laboratory of Rare Earth Materials Chemistry and Applications, College of Chemistry and Molecular Engineering, Peking University, Beijing 100871, P.R. China*

List of contents:

1. **Experimental section.**

2. **Supplementary equations.**

3. **Supplementary figures.**

4. **Supplementary tables.**

1. Experimental section.

Synthesis of $SrOCuBiSe_2$ Single Crystals. Single crystals of $SrOCuBiSe_2$ were synthesized by the salt-melt method. A mixture of 1 mmol SrSe powder, 1 mmol Bi powder, 1 mmol CuO powder, 1 mmol Se powder and 5 mmol CsI was ground and loaded into carbon-coated fused silica tubes under an Ar atmosphere in a glovebox, which was flame-sealed under vacuum (10^{-3} mbar). The tubes were heated to 1053 K in 12 h and kept at the temperature for 50 h, then cooled at a rate of 2 $K \cdot h^{-1}$ to 873K. Then the furnace was turned off to cool the tube to room temperature. Black block-shaped crystals were obtained by breaking the tubes.

Synthesis of $SrOCuBiSe_2$ Powder. Powder of $SrOCuBiSe_2$ was synthesized by solid-state reaction of stoichiometric amount of SrSe, CuO, Bi powders and Se powders in a sealed carbon-coated fused-silica tube evacuated to 10^{-3} mbar. The tubes were heated to 913K in 6 h and kept at this temperature for 2 days. Then the furnace was turned off to cool the tube to room temperature. The final powder was densified in a spark plasma sintering (SPS) furnace in a graphite die (Φ 10mm) under a pressure of 60 MPa at 873 K, held for 5 min in argon atmosphere. The obtained pellets had relative densities larger than 95% of the theoretical value (6.831 g/cm^3).

Single-Crystal X-ray Crystallography. Suitable crystals were chosen to perform the data collections. Single crystal X-ray diffraction was performed on a Bruker D8QUEST diffractometer equipped with Mo $K\alpha$ radiation. The diffraction data were collected at room temperature by the ω- and φ- scan methods. The crystal structures were solved and refined using APEX3 program. Absorption corrections were performed using the multi-scan method (ASDABS).[1] The detailed crystal data and structure refinement parameters and fractional atomic coordinates parameters are summarized in Table S2-S3 in Supporting Information.[1]

Characterization. The obtained crystals were investigated with a JEOL (JSM6510) scanning electron microscope equipped with energy dispersive X-ray spectroscopy (EDXS, Oxford Instruments). Powder X-ray diffraction of the samples were collected

on a Bruker D8QUEST diffractometer equipped with mirror-monochromated Cu *Kα* radiation (λ= 0.15406 nm). The patterns were recorded in a slow-scanning mode with 2ϑ from 10° to 80° at a scan rate of 2°/min. Simulated patterns were generated by using the MERCURY program and CIF file of the refined single crystal structure. The solid-state ultraviolet-visible (UV-vis) light diffuse-reflectance spectra of the fine powders were measured on a UV-4100 spectrophotometer operating from 1200 to 350 nm at room temperature. $BaSO_4$ powder was used as a 100% reflectance standard. The powder sample was spread on a compacted base of $BaSO_4$ powder. The generated reflectance-versus-wavelength data were used to measure the band gap of the as-synthesized samples. The reflectance data were converted to absorbance data by using the Kubelka-Munk equation.[2]

Thermal Analyses. Thermogravimetric analysis (TG) and differential scanning calorimeter (DSC) were carried out on a NETZSCH STA449C thermal analyzer for investigating the thermal properties of the $SrOCuBiSe_2$ compound. A well-ground powder sample was loaded into an Al_2O_3 crucible and heated from room temperature to 950 °C at 10 °C/min under a constant flow of argon gas.

Transport Property Measurement. The high temperature (300−850 K) electrical resistivity (ρ) and Seebeck coefficient (S) were simultaneously measured using an ULVAC-RIKO ZEM 3 apparatus. For this measurement, bar samples about 1.5 mm×2 mm×10 mm were used. Electrical conductivity was measured by a four-probe method. Thermoelectromotive force (ΔE) at the test temperature was measured using five different temperature gradients ($0 < \Delta T < 2$ K) to calculate the Seebeck coefficient from the ΔE versus ΔT plot. Thermal diffusivity coefficient λ was determined using a laser-flash method in a flowing Ar atmosphere (Netzsch LFA 427). The thermal conductivity was calculated from $k = C_p\rho\lambda$, where ρ is the density and C_p is the specify heat capacity. The C_p is estimated using the Dulong-Petit model ($C_p = 3k_b/atom$), which matches well with the experimental results. The Wiedemann-Franz law, using a Lorentz number of 1.5×10^{-8} W·Ω·K^{-2}, was used to calculate the lattice thermal conductivity by subtracting

the electronic contribution from the total thermal conductivity ($k_L = k - k_e$). Room-temperature Hall effect (-2 T−2 T) was measured using a Physical Properties Measurements System (PPMS−Quantum Design Dyna Cool). The formula $p = 1/R_H e$, was used to calculate the carrier concentration by the approximation of single parabolic band conduction model (Table S4).

Electronic Structure Calculation. First principles calculations were performed using the Vienna Ab Initio Simulation Package (VASP).[3-5] The Perdew-Burke-Ernzehof (PBE) version of the generalized gradient approximation (GGA) was used to describe the exchange correlation functional, and the projector augmented wave (PAW) method was used in the present work.[6] Here the cutoff energy of plane wave was chosen at 480 eV. For the structure optimizations, 6×10×5 k-points were used for the conventional cell. The convergence criteria were that the change in total energies between two successive electronic steps was less than 10^{-5} eV, and all the Hellmann-Feynman force acting on each atom was less than 0.01 eV /Å. High-symmetry points in Brillouin zones (X, Γ, Z, B, and A represent (0.5, 0.5, 0), (0, 0, 0), (0, 0.5, 0), (0, 0, 0.5), and (-0.5, 0, 0.5)) were considered in our band structure calculation.

To understand the bonding character in $SrOCuBiSe_2$, we calculated the electron localization function (ELF). The ELF can be expressed as $ELF(\mathbf{r}) = \{1 + [K(\mathbf{r})/Kh(\rho(\mathbf{r}))]^2\}^{-1}$, where K is the curvature of the electron pair density for electrons of identical spin, $\rho(\mathbf{r})$ is the density at $\mathbf{r}$, and $Kh[\rho(\mathbf{r})]$ is the value of K in a homogeneous electron gas with density ρ. The ELF has often been used to characterize the degree of electron localization to quantitatively identify the character of chemical bonds between atoms. The ELF value lies by definition between zero and 1. ELF = 0 corresponds to no localization (regions without any electron), ELF = 0.5 reflects the behavior of a homogeneous electron distribution (as found in regions where the bonding has a metallic character), and ELF = 1 indicates full localization (as found in regions of covalent bonds, core shells, and lone pairs).

Phonon calculations. To study the lattice dynamics of $SrOCuBiSe_2$, phonopy as interfaced with VASP was used to calculate the phonon properties based on finite

displacement methods.[7-8] A supercell with dimensions of 2×4×2 (including 192 atoms) was constructed. High-symmetry points in the Brillouin zone (X, Γ, Y, S, R, T, and Z represent (0.5, 0, 0), (0, 0, 0), (0, 0.5, 0), (0.5, 0.5, 0), (0.5, 0.5, 0.5), (0, 0.5, 0.5), and (0, 0, 0.5)) were considered in our phonon dispersion and Grüneisen parameter calculations.

2. Supplementary equations.

The effective mass m^* is estimated according to the following equation using the observed carrier concentration (n_h) and Seebeck coefficient (*S*) values:[9-10]

$$m^* = \frac{h^2}{2k_BT}\left[\frac{n}{4\pi F_{1/2}(\eta)}\right]^{\frac{2}{3}} \qquad (1)$$

$$S = \pm\frac{k_B}{e}\left(\frac{(r+3/2)F_{r+3/2}(\eta)}{(r+3/2)F_{r+1/2}(\eta)} - \eta\right) \qquad (2)$$

$$F_n(\eta) = \int_0^\infty \frac{\chi^n}{1+e^{\chi-\eta}}d\chi \qquad (3)$$

Where η is the reduced Fermi energy, $F_n(\eta)$ is the nth order Fermi integral, k_B is the Boltzmann constant, *e* is the electron charge, *h* is the Planck constant and *r* is the scatting factor. The scattering factor (*r*) is -1/2 as the acoustic phonon scattering is independent of the grain size and is generally assumed to be the main scattering mechanism at room temperature.

The lattice thermal conductivity (k_L) values were estimated by subtracting the carrier thermal conductivity (k_e) from the total *k*:

$$k_L = k - k_e \qquad (4)$$

Where the Wiedemann-Franz relation with a Lorenz constant of $L_0 = 1.58 \times 10^{-8}$ $V^2 \cdot K^{-2}$ is applied for estimating k_e:[11]

$$k_e = L_0\sigma T \qquad (5)$$

3. Supplementary figures.

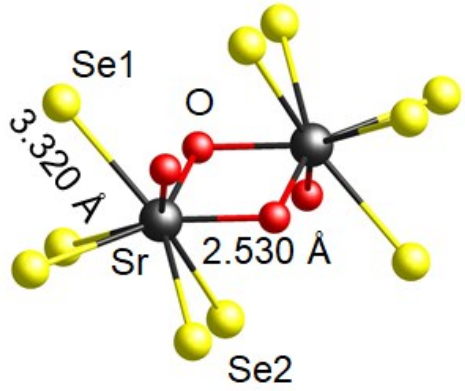

Figure S1. Coordination the polyhedra of the Sr cations in $SrOCuBiSe_2$.

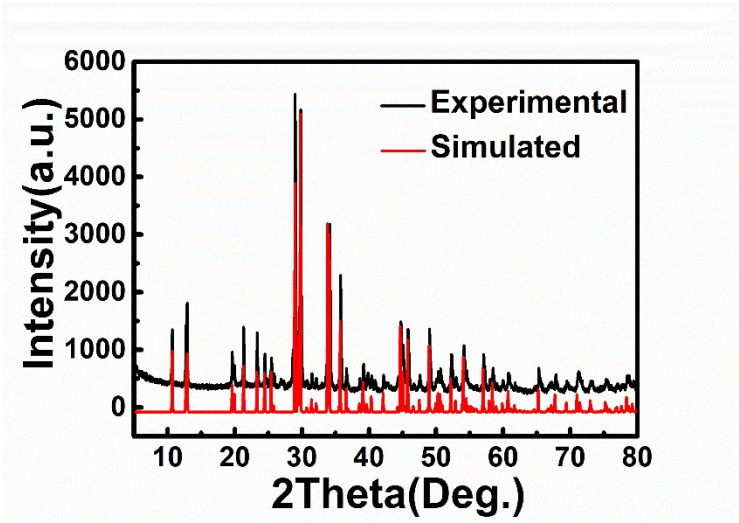

Figure S2. The PXRD patterns of $SrOCuBiSe_2$. The simulated patterns were generated (red line) based on the CIF files.

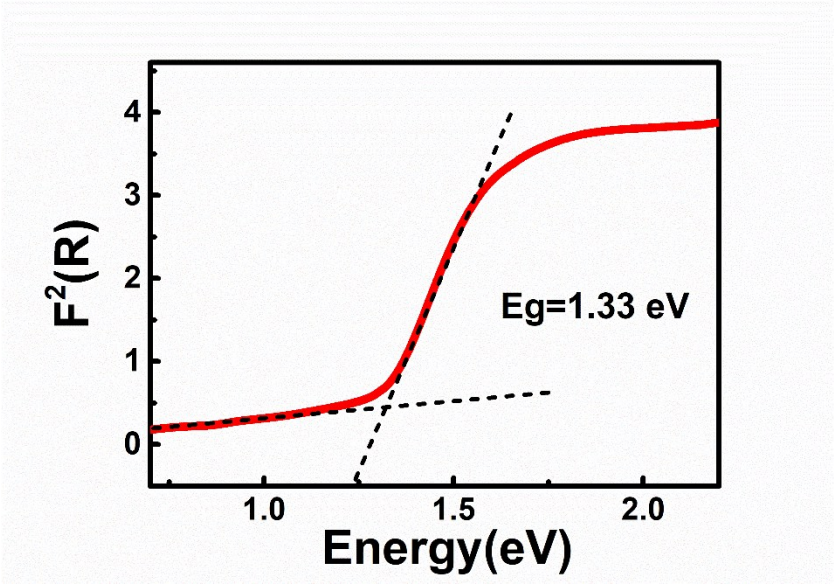

Figure S3. The plot of $F^{1/2}(R)$ *vs* energy for the absorption spectra of $SrOCuBiSe_2$. (Insert) The solid-state UV-Vis-NIR absorption spectra of $SrOCuBiSe_2$.

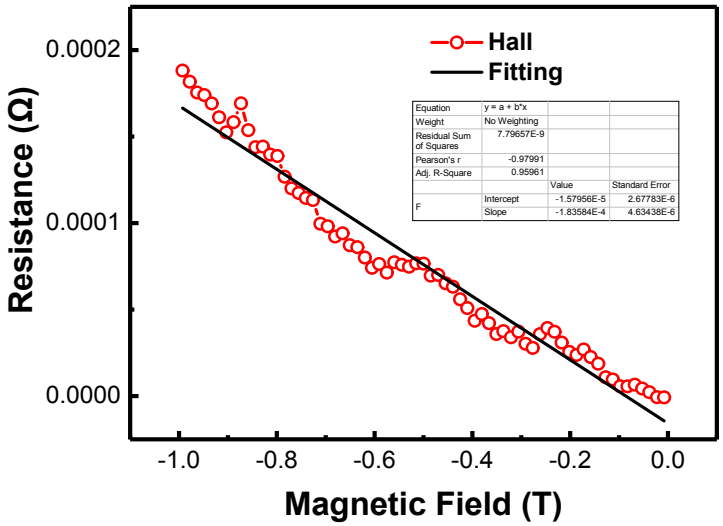

Figure S4. Hall coefficient measurements of $SrOCuBiSe_2$.

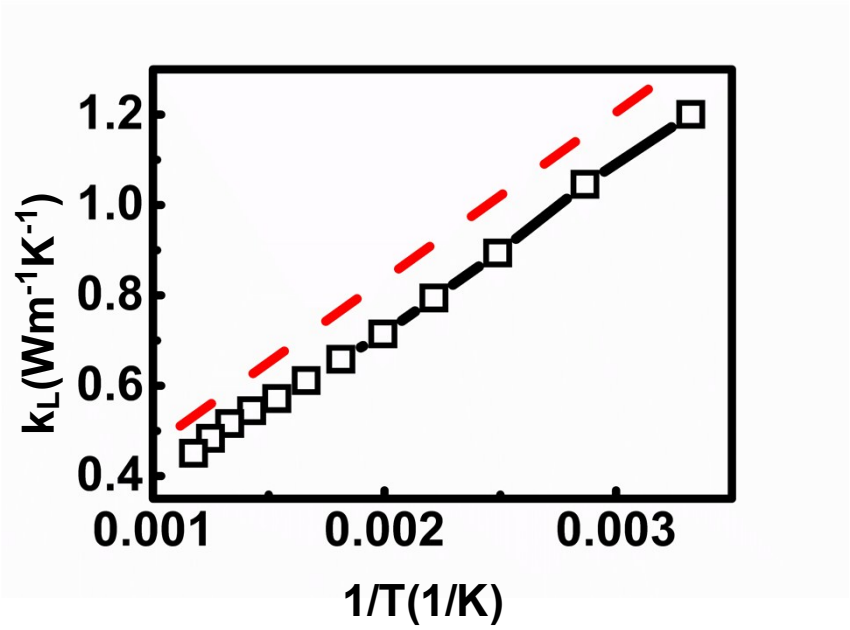

Figure S5. lattice thermal conductivity (κ_L) and the relationship of $\kappa_L \propto T^{-1}$ (inset) in the $SrOCuBiSe_2$.

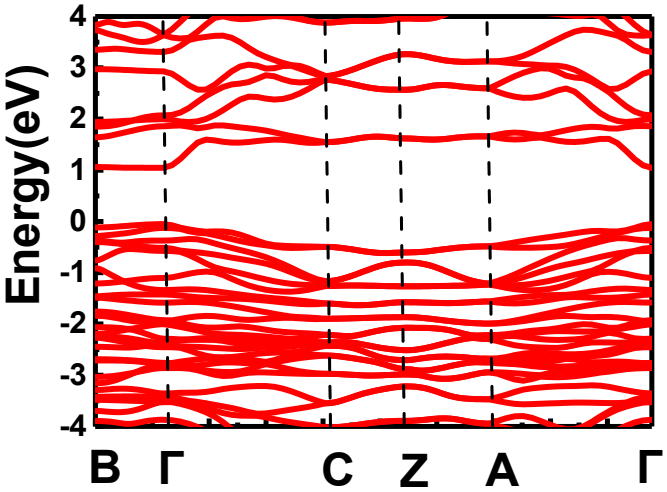

Figure S6. The band structure of $SrOCuBiSe_2$.

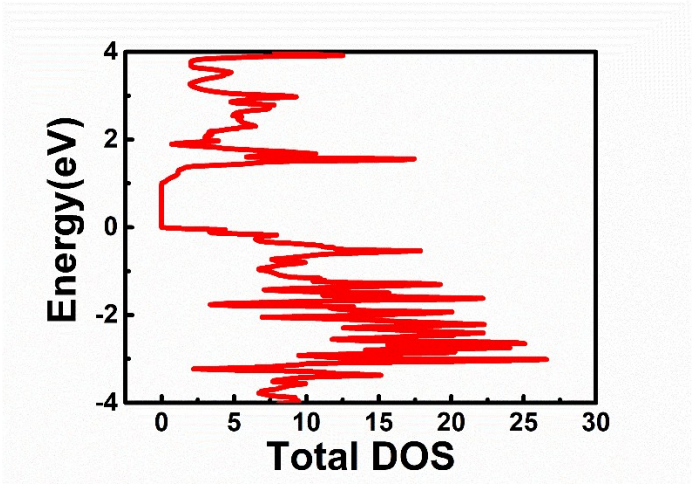

Figure S7. The total DOS of $SrOCuBiSe_2$.

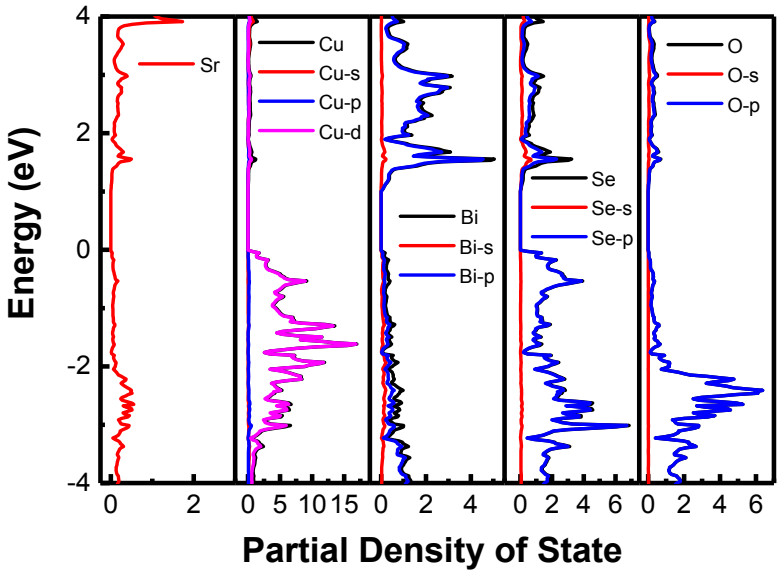

Figure S8. The partial DOS of $SrOCuBiSe_2$.

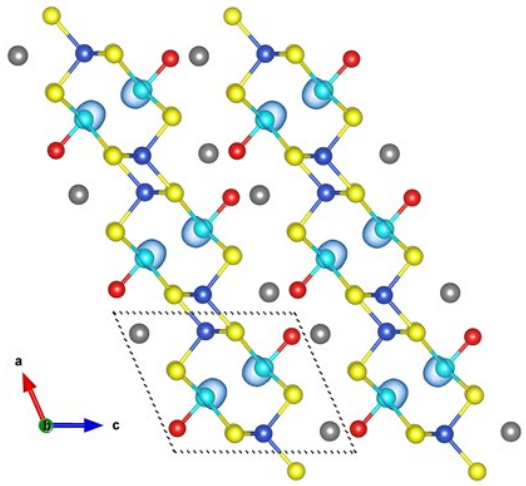

Figure S9. The ELF graph of the $SrOCuBiSe_2$.

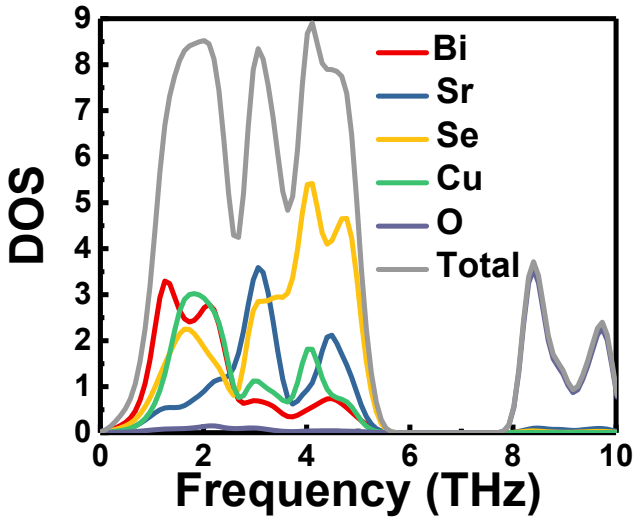

Figure S10. Total and projected phonon density of states of different atoms.

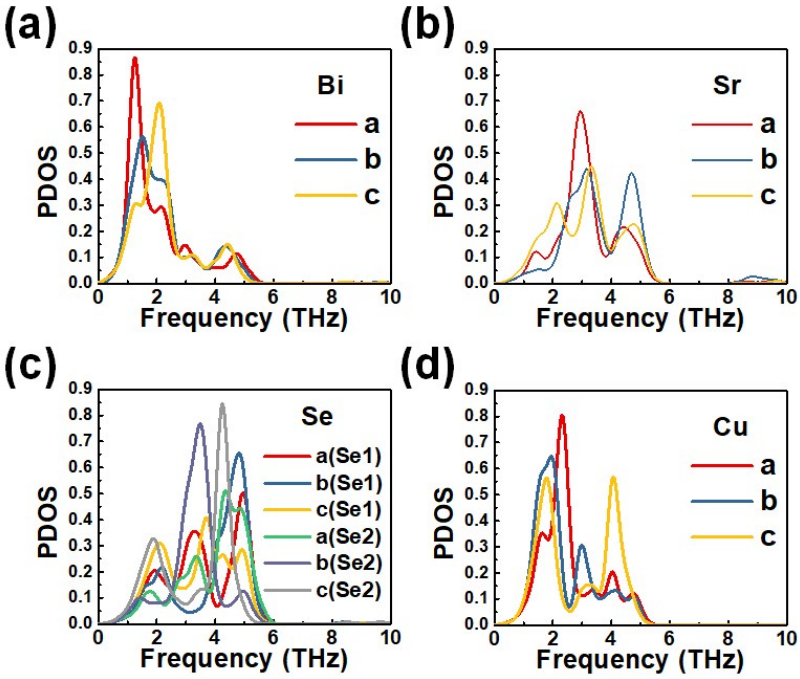

Figure S11. Partial DOS for (a) Bi, (b) Sr, (c) Se and (d) Cu atoms in different orientations.

4. Supplementary tables.

Table S1. Crystal Data and details of the structure refinements for $SrOCuBiSe_2$.

Chemical formula	$SrOCuBiSe_2$
F_w (g·mol^{-1})	534.06
Crystal system	Monoclinic
Space group	C_{2h}^{2}-$P2_1/m$ (No. 11)
a (Å)	7.6529(5)
b (Å)	4.0559(3)
c (Å)	9.1405(6)
β (deg)	113.758(2)
V (Å^3)	259.67(3)
Z	2
Crystal color	Black
ρ_c (g·cm^{-3})	6.830

μ (mm^{-1})	61.95
F(000)	452
R_{int}	0.027
R_1 [$I > 2\sigma(I)$]	0.044
wR_2 (all data)	0.109
GOF	1.16

[a]$R_1 = \sum||F_o| - |F_c||/\sum|F_o|$. [b]$wR_2 = \{\sum[w(F_o^2 - F_c^2)^2]/\sum[w(F_o^2)^2]\}^{1/2}$, $w = 1/[\sigma^2(F_o^2) + (0.1000P)^2]$, where $P = (F_o^2 + 2F_c^2)/3$.

Table S2. Atomic coordinates and isotropic displacement parameters (Å^2) of the $SrOCuBiSe_2$ compound refined from single X-ray diffraction data recorded at room temperature.

atom	site	occ	x	y	z	U_{iso}*/U_{eq}
Bi	2e	1	0.60919 (7)	1.25	0.70314 (5)	0.0397 (4)
Sr	2e	1	0.85222 (19)	0.75	1.09067 (17)	0.0386 (4)
Se1	2e	1	0.1330 (2)	0.25	0.37230 (18)	0.0396 (4)
Se2	2e	1	0.4188 (2)	0.75	0.79739 (16)	0.0398 (4)
Cu	2e	1	0.1380 (3)	0.75	0.5372 (2)	0.0501 (6)
O	2e	1	0.8306 (14)	1.25	0.9285 (11)	0.0393 (19)

Table S3. Carrier concentration n_h, hall mobility μ_h and effective mass m* of $SrOCuBiSe_2$ at room temperature.

n_h (10^{19} cm^{-3})	μ_h (cm^2 V^{-1} s^{-1})	m^*
2.389	0.1137	$1.50m_0$

Table S4. Debye temperatures (θ), group velocities (v), and Grüneisen parameters (γ) for the $SrOCuBiSe_2$ compounds.

	$SrOCuBiSe_2$		
	TA	TA'	LA
ϑ(K)	60	64	78
υ(m/s)	1735	1951	3949
γ	3.746	3.529	3.097

Table S5. Anisotropic displacement parameters (Å^2) of the Cu atoms.

	U11	U22	U33

$SrOCuBiSe_2$	0.050 (1)	0.052(1)	0.050 (1)
$CuBiSe_2$	0.0216(3)	0.0216(3)	0.0188(3)
$CuBiS_2$	0.033(1)	0.033 (2)	0.021(1)

Reference：

1. G. Sheldrick, *Acta Crystallogr., Sect C.* 2015, **71**, 3-8.

2. G. Kortüm, W. Braun, G. Herzog, *Angew. Chem. Int. Ed.* 1963, **2**, 333-341.

3. G. Kresse, Hafner, *J. Phys. Rev. B.* 1993, **47**, 558-559.

4. G. Kresse, Furthmüller, *J. Comput. Mater. Sci.* 1996, **6**, 15-50.

5. G. Kresse, Furthmüller, *J. Phys. Rev. B.* 1996, **54**, 11169-11186.

6. J. P. Perdew, K. Burke, *Phys. Rev. Lett.* 1996, **77**, 3865-3868. 7. K. Parliñski, *Materials Design,* 2005.

8. K. Parlinski, Z. Li, Y. Kawazoe, *Phys. Rev. Lett.* 1997, **78,** 4063-4066.

9. K. Wojciechowski, M. Schmidt, *Phys. Rev. B,* 2009, **79,** 184202.

10. S. N. Guin, A. Chatterjee, D. S. Negi, R. Datta, K. Biswas, *Energy Environ. Sci.* 2013, **6,** 2603-2608.

11. H. Takahashi, N. Raghavendra, F. Gascoin, D. Pelloquin, S. Hébert, E. Guilmeau, *Chem. Mater.* 2013, **25,** 1809-1815.